On the emplacement of the impact melt breccia at the Dhala Impact structure, India.

Gaurav Joshi[1], Pradyut Phukon[1], Amar Agarwal[1], and Arun Kumar Ojha[2]

[1]Indian Institute of Technology Kanpur
[2]CSIR-National Geophysical Research Institute

February 22, 2024

Abstract

We investigate the magnetic fabrics of Impact melt breccia at the Dhala impact structure to understand its emplacement mechanism. Our results show that the pseudo-single domains of Ti-poor magnetite and Ti-hematite are the prime magnetic carriers in the impact melt breccia. The magnetic fabrics from most sites reveal a general westward flow of impact melt breccia (IMB), with magnetic lineations of individual specimens trending between NW and SW. This indicates the emplacement of IMB in a semi-molten state with temperatures below c. 1500°C, which is the melting point of Ti-magnetite. Occurrence of poorly sorted clasts implies that IMB was emplaced as surficial flow rather than aerial. The variation in the dips of magnetic fabrics among individual specimens from a site resembles a pyroclastic flow rather than a ground-hugging volatile- and melt-rich flow. We, therefore, suggest that the IMB at Dhala was ballistically ejected and then moved in a semi-molten state as surficial pyroclastic-like flow with temperatures below c. 1500°C. Most flow vectors aligned between NW-SW, may represent a dominant westward excavation flow of the IMB (rather than radially outward flow), which may be activated by an east-to-west directed impactor striking at an impact angle below 50°.

On the emplacement of the impact melt breccia at the Dhala Impact structure, India.

Gaurav Joshi[1], Pradyut Phukon[1], Amar Agarwal[1], and Arun Kumar Ojha[2]

[1]Department of Earth Sciences, Indian Institute of Technology-Kanpur, Kanpur, 208016, India.

[2]CSIR-National Geophysical Research Institute, Hyderabad, 500007, India

Corresponding author's email: gjoshi@iitk.ac.in

Abstract

We investigate the magnetic fabrics of Impact melt breccia at the Dhala impact structure to understand its emplacement mechanism. Our results show that the pseudo-single domains of Ti-poor magnetite and Ti-hematite are the prime magnetic carriers in the impact melt breccia. The magnetic fabrics from most sites reveal a general westward flow of impact melt breccia (IMB), with magnetic lineations of individual specimens trending between NW and SW. This indicates the emplacement of IMB in a semi-molten state with temperatures below c. 1500°C, which is the melting point of Ti-magnetite. Occurrence of poorly sorted clasts implies that IMB was emplaced as surficial flow rather than aerial. The variation in the dips of magnetic fabrics among individual specimens from a site resembles a pyroclastic flow rather than a ground-hugging volatile- and melt-rich flow. We, therefore, suggest that the IMB at Dhala was ballistically ejected and then moved in a semi-molten state as surficial pyroclastic-like flow with temperatures below c. 1500°C. Most flow vectors aligned between NW-SW, may represent a dominant westward excavation flow of the IMB (rather than radially outward flow), which may be activated by an east-to-west directed impactor striking at an impact angle below 50°.

Key Points:

The general westward trend of magnetic lineations indicates that the IMB flowed towards the west.

IMB moved in a semi-molten state as surficial pyroclastic-like flow with temperatures below c. 1500°C.

The westward excavation flow of the IMB may be activated by an east-to-west directed impactor striking at an impact angle below 50°.

Plain Language Summary

The study of impact melts concerning their composition, distribution, emplacement, etc., is very common in extra-terrestrial craters. However, on Earth, impact melts are not well preserved because of weathering and erosion and are poorly understood. Here, we investigate the magnetic fabrics of IMB at the

Dhala impact structure to understand its emplacement mechanism. The rock magnetic studies reveal a general westward flow of IMB having Ti-poor magnetite and Ti-hematite as the primary magnetic carriers. This implies that the IMB was in a semi-molten state during the emplacement having temperatures below c. 1500°C (melting point of Ti-magnetite). The presence of poorly sorted clasts suggests that IMB was emplaced as surficial flow rather than aerial, and the variation in the dips of magnetic fabrics among individual specimens from a site resembles a pyroclastic-like flow. Therefore, we suggest that the IMB at Dhala was ballistically ejected and then moved in a semi-molten state as surficial pyroclastic-like flow with temperatures below c. 1500°C. The dominant westward excavation flow of the IMB was possibly initiated by an east-to-west directed impactor striking at an impact angle less than 50°.

Keywords: Impact melt Breccia, Dhala Impact Structure, Magnetic fabrics, Flow direction, Pyroclastic flow, Impact direction.

Introduction

Meteoritic impact events associated with crystalline or mixed crystalline crust in the basement produce impact melt (Osinski, 2004). The kinetic energy transfer from bolide into the target rock causes brecciation and decompression melting of the target rock (Dressler and Reimold, 2001; Sugandhi and Agarwal, 2022). Most impact melts are found in and around impact structures as crater-fill deposits, sheet-like bodies, smaller isolated patches, veins, dykes, and melt fragments in allochthonous breccias (Dressler and Reimold, 2001; French, 1998; Osinski, 2004).

Investigations of terrestrial and extra-terrestrial impact melt have proven to be critical in understanding impact cratering related processes such as direction of impact, age of the crater, weathering intensity, geochemical identification of the impactor, subsurface mineralogy, etc. (e.g., Barlow, 2010; Mader and Osinski, 2018; Osinski, 2004; Osinski et al., 2011; Pierrazzo and Melosh, 2000; Siegert et al., 2017; Stöffler et al., 2004; Stopar et al., 2014). Furthermore, impact melts injected into the crater subsurface act as a heat source for hydrothermal systems (e.g., Osinski et al., 2020, 2013). These systems may remain active for thousands of years after the impact event and may act as a cradle for new life and develop economically viable ore deposits (e.g., Grieve, 2005; Kring, 2000; Osinski et al., 2020, 2013; Reimold et al., 2005). Although the impact melts are very common at extra-terrestrial craters, on terrestrial craters, the impact melts are often completely erased by erosion.

The Dhala impact structure (Fig. 1) was formed during Paleoproterozoic times in the Archean crystalline basement of the Bundelkhand Craton (Pati et al., 2010, 2008). Within the Dhala impact crater, there are seven outcrops of IMB. Over the past fifteen years, the shock deformation structures, lithology, radiometric dating, petrology, and geochemistry have been well defined (e.g., Agarwal

et al., 2020; Pati et al., 2019, 2017, 2015, 2010, 2008; Singh et al., 2021a, 2021b). However, the emplacement setting of the IMB, such as its flow direction, aerial vs. surface flow, lamellar (melt and volatile-rich) or turbulent flow (like pyroclastic), and its solid or fluid state during emplacement, is not well established. Although Singh et al. (2021a) investigated the flow directions in IMB, they did not find any consistent trend. To determine the emplacement setting of the IMB, the present study investigated magnetic fabrics and compared them with mesoscopic flow indicators.
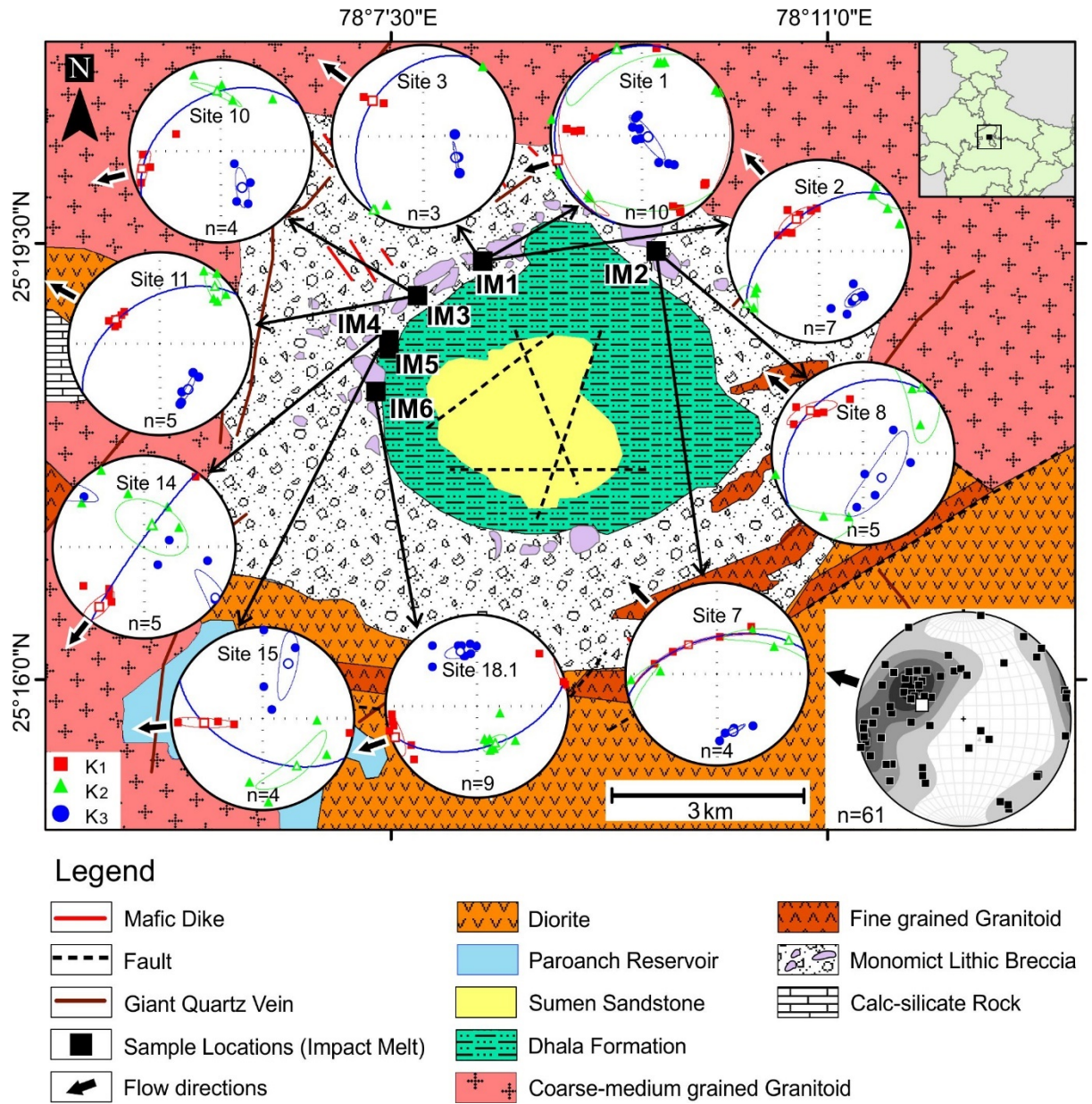
Figure 1: Geological map of the Dhala impact structure (after Pati et al., 2008) presenting major lithologies, impact melt breccia outcrops, and sample locations. Stereonets demonstrate the principal susceptibility axes (K_1, K_2, K_3) distribution with their corresponding means (open symbols) and confidence ellipses from individual sites. The inferred flow direction is marked by black arrow. Inset: Overall flow direction (black arrow) inferred from cumulative distribution of K_1

of all sites.

Magnetic fabrics studies are a very well-established technique to determine the flow direction in volcanic and fluvial deposits (e.g., Alva-Valdivia et al., 2017; Cañón-Tapia et al., 1997, 1996, 1995; Guimarães et al., 2018; Liu et al., 2001; Papanna et al., 2014; Tarling, D.H., and Hrouda, 1993). This is because the magnetic carriers align themselves along the flow direction due to the viscous drag, rendering a preferred orientation of the magnetic fabrics (e.g., Cañón-Tapia and Mendoza-Borunda, 2014; Tarling and Hrouda, 1993). Most studies have shown that mean K_1 is parallel with the flow directions (e.g., Cañón-Tapia and Castro, 2004; Cañón-Tapia et al., 1996, 1995; Guimarães et al., 2018); and relatively lesser number of studies have shown the parallelism of either mean K_2 (e.g., Ellwood, 1978; Khan, 1962); or mean K_3 with the flow direction (e.g., Alva-Valdivia et al., 2017; Gil-Imaz et al., 2006). In each of these cases, the alignment of different principal magnetic susceptibility axes with the flow direction is owed to the mineralogy and the domain size of the magnetic carriers. Thus, before interpreting the flow directions in an area, it is crucial to characterize the magnetic mineralogy and domain size, and to compare the orientation of the susceptibility axes with the geological flow indicators like elliptical vesicles, alignment of the lithic clasts, etc., wherever available (Agarwal et al., 2016; Cañón-Tapia and Castro, 2004; Cañón-Tapia et al., 1995; MacDonald and Palmer, 1990).

In the present study, we investigate the flow directions of IMB at all six outcrops. Larger outcrops have more than one sampling site to average out local variations, such that we have a total of 11 sampling sites (Fig. 1, Table 1). We combined magnetic fabric results from these 11 sites and the mesoscopic flow indicators from 5 sites (10 specimens) to infer the flow direction and emplacement of the impact melt breccia.

Table 1: Summary of rock magnetic results. N- number of cores. K_m- mean bulk susceptibility, P'- corrected degree of magnetic anisotropy, and T- shape factor of AMS ellipsoid. Int- intensity, D°- declination, I°- inclination, and Conf°- confidence angles of the maximum (K_1) and minimum (K_3) principal susceptibility axes. See supplementary table 1 for individual specimens.

Outcrop	Site	N	K_m (10⁻³ SI)	P'	T	K_1				K_3	
						Int.	D°	I°	Conf°	Int.	D°
IM1	Site 1	10	0.692	1.020	0.705	1.005	254.2	4.5	51.7/7.0	0.991	105
	Site 2	7	0.602	1.015	0.398	1.006	325.2	54.5	18.6/6.4	0.992	142
	Site 3	3	0.689	1.012	-0.462	1.007	305.3	33.3	9.1/0.0	0.995	120
IM2	Site7	4	0.682	1.020	0.392	1.006	315.2	53.2	59.9/1.4	0.989	165
	Site 8	5	0.805	1.014	0.139	1.005	309.4	26.8	22.7/6.4	0.995	143
IM3	Site 10	4	0.938	1.020	0.591	1.007	257.1	13.5	15.8/5.1	0.990	149
	Site11	5	1.085	1.020	-0.081	1.010	298.2	45.3	6.7/4.0	0.991	147

Outcrop	Site	N	K_m (10^{-3} SI)	P'	T	K_1				K_3	
IM4	Site 14	5	0.889	1.015	0.317	1.005	217.1	19.4	21.3/5.4	0.995	12
IM5	Site 15	4	1.724	1.006	0.023	1.002	265.8	35.6	31.3/3.7	0.998	25.
IM6	Site 18.1	9	1.862	1.015	0.088	1.006	249.7	4.3	13.6/9.6	0.993	342
	Site 18.2	5	1.403	1.005	-0.060	1.001	128.9	68.3	21.6/9.7	0.997	344

Geological setting

The Paleoproterozoic Dhala impact structure (c. 2.5 to 1.7 Ga old) is located in the Shivpuri district of Madhya Pradesh, India (N25°17'59.7" and E78°08'3.1"). It was identified as an eroded remnant of the impact crater based on a variety of shock deformation features (Pati et al., 2008). It is the largest and oldest impact structure currently known in the Indian subcontinent, covering 64 km^2 area and 11 km in diameter (Pati et al., 2017, 2008). The topography of the area is gradually undulating, with a prominent, flat-topped central elevated area in the central part (Fig. 1). The crystalline basement of the Bundelkhand craton formed the target lithology and is mainly composed of granitoids (2563 $\pm$ 6 Ma age) with a 12.36 m thick suevite horizon (Pati et al., 2019). It is overlain by IMB comprising clasts of quartz, feldspar, zircon, and some opaque mineral together with larger fragments of partially to completely melted target granitoid (Pati et al., 2019; Singh et al., 2021a). The clasts are embedded in a fine-grained matrix of mainly quartz and feldspar. The IMB shows signs of post-impact hydrothermal alteration like sericitization, chloritization, etc. (Pati et al., 2017, 2010). A 1.8 m thick layer of suevite occurs above the IMB.

The suevite is unconformably overlain by sediments of the Dhala Formation, which is equivalent to the Semri Group of the Vindhyan Supergroup (Pati et al., 2019). It comprises interbanded arkosic sandstone, grit, siltstone, shales, and conglomerate pockets, with synsedimentary deformation structures (Reddy et al., 2015). The depositional age of the Dhala Formation is c. 1.7 Ga (Ray et al., 2003; Sarangi et al., 2004), which indicates the impact event occurred between 1.7-2.5 Ga (Pati et al., 2010). The rocks of the Dhala Formation are unconformably overlain by Kaimur sandstone (Sumen sandstone) belonging to the Kaimur Group of the Vindhyan Supergroup. It is partially covered by lateritized conglomerate.

The Dhala impact structure contains monomict lithic breccia that covers about 45 km^2 in the outermost annular zone of the structure. Along the inner margin of this monomict lithic breccia unit, patchy outcrops of IMB (2.4 km^3) occur over a distance of about 6 km in a semi-circular pattern between the villages of Maniar and Pagra (Pati et al., 2015, 2008).

Methodology

To analyze the microscopic and magnetic properties of the IMB, we obtained 46 oriented cylindrical drill cores (1'' in diameter and 4-5'' long) from 11 rock magnetic sites using a portable hand drill. To assess the local variations in the flow directions within each outcrop, large IMB outcrops were divided into two to three rock magnetic sites (Table 1). The location of the IMB was selected from the earlier reports (e.g., Pati et al., 2019, 2017, 2008), and all the drill cores were collected from the rocks where the melt was free from the large clasts. We avoided fractured and weathered outcrops. The cylinders were oriented using a magnetic compass before being removed from the rocks. The cylinders were cut into specimens (61 nos.), which are 2.54 cm in diameter and 2.2 cm in length.

Magnetic fabrics analyses

Anisotropy of magnetic susceptibility (AMS) was measured for each core using KLY-4S Kappabridge of AGICO (Brno, Czech Republic) at the Department of Geology and Geophysics, Indian Institute of Technology, Kharagpur, India. Standard rock magnetic parameters, namely, the mean bulk susceptibility (K), corrected degree of magnetic anisotropy (P'), and mean of the shape factor of AMS ellipsoid (T), were obtained using Anisoft- 5.1.08 (Chadima and Jelinek, 2009; Tarling and Hrouda, 1993). The orientations of principal susceptibility axes, K_1 K_2 K_3, were calculated from their respective declination (D°) and inclination (I°). The K_1 axis and the K_1 K_2 plane represent the magnetic lineation and the magnetic foliation, respectively. The magnitudes of the principal susceptibilities are used to calculate the mean susceptibility (K_m), the corrected degree of magnetic anisotropy (P'), and the shape parameter (T) according to the Eqs. (1) – (3) (after Tarling and Hrouda, 1993; Jelínek and Kropáček, 1978). Dispersion in K_1 and K_3 at each site is represented by the confidence angles (after Jelínek and Kropáček, 1978). The data were processed, and the mean was calculated through Anisoft- 5.1.08 (Chadima and Jelinek, 2009; Tarling and Hrouda, 1993).

$$K_m = K_1 + K_2 + K_3/3 \ (1)$$

$$P' = exp.[\{2[(\eta_1 - \eta_m)^2 + (\eta_2 - \eta_m)^2 + (\eta_3 - \eta_m)^2]\}^{1/2}] \ (2)$$

$$T = (2\eta_2 - \eta_1 - \eta_3)/(\eta_1 - \eta_3) \ (3)$$

Here, $\eta_1 = \ln K_1$, $\eta_2 = \ln K_2$, $\eta_3 = \ln K_3$ and $\eta_m = (\eta_1 \cdot \eta_2 \cdot \eta_3)^{1/3}$.

Thermomagnetic measurements

Temperature-dependent low field magnetic susceptibility measurements have been done using a Kappabridge (KLY-4S), equipped with a CS-3 furnace and a

CS-L cryostat, between temperatures of -194 °C and a maximum of 700°C at the Department of Applied Geology, Karlsruhe Institute of Technology, Germany.

The measurements were carried out in two parts. In the first part, the samples were cooled using liquid nitrogen to -194°C, and the bulk susceptibilities of the samples were measured as they gradually warmed up to room temperature. The liquid nitrogen was flushed out using blasts of argon. In the second part, the samples were heated at a rate of 10°C/min up to 700°C and then cooled back to room temperature. The bulk susceptibility was measured during the entire cycle of heating and cooling. Possible oxidation of the sample while heating was minimized by flushing out air from the sample holder using argon flowing at 50 ml/min.

Measurement of magnetic hysteresis

Hysteresis curves were obtained using a vibrating sample magnetometer (VSM) at Advanced Center for Material Science (ACMS), IIT Kanpur, in a field up to 1.8 Tesla. A MATLAB-based software called HystLab (Paterson et al., 2018) was used for the paramagnetic correction and to calculate the coercive force (Hc), the remanent-magnetization (Mrs), and saturation-magnetization (Ms). Remanent coercivity (Hcr) was calculated using the method elucidated by (Tauxe et al., 1996). The Hcr/Hc and Mrs/Ms ratios were plotted on the Day plot to estimate the relative proportions of the single domain (SD), multi-domain (MD), and pseudo-single domain (PSD) grains (Dunlop, 2002a, 2002b).

Microscopy

After the AMS measurements, at least one oriented thin section from each site was prepared using the cylindrical specimens. Transmitted and reflected light microscopy, done on a Leica DM2700P microscope, revealed the magnetic mineralogy and different shock deformation features.

1.

Results

(a)

Outcrop and microscopic features

A couple of IMB outcrops (IM2 and IM3) are small hillocks, 5-20 meters high, while IM1 and IM6 are larger outcrops (over 50 m^2), which can be easily distinguished from the surrounding fractured monomict breccia. IM4 and IM5 are

merely weathered remnants with small outcrops protruding just a few decimetres above the ground. IMB outcrops are reddish to orange in colour and are marked with circular to elliptical-shaped vesicles (Figs. 2a, b). These vesicles are millimetre to centimetre in size and are sometimes filled with secondary minerals such as agate, quartz, calcite, chlorite, and smectite.

IMB comprises quartz, feldspar, and opaque mineral grains in a very fine-grained matrix. The rock shows the presence of poorly sorted clasts of the basement granite in thin sections (Fig. 2c) and contains vesicles in both the clasts and the melt matrix. IMB exhibits remarkable flow texture under thin sections (Fig. 2d) and a general impression of fluidal domains of recrystallized feldspar, quartz, and some opaque minerals. Armoured lapillies are common in IMB (Fig. 2e) and are also reported from other impact structures (e.g., Lonar, Ries, Sudbury, Bosumtwi, and Chicxulub impact structures). The shock metamorphism is represented in the form of planar deformation features (PDFs) in quartz (Fig. 2f). One to two sets of decorated PDFs are observed at IM2 and IM3.

Cubic and skeletal Ti-magnetite is the primary magnetic carrier (Figs. 2g, h, and i). A sample exhibits either skeletal or cubic grains, never both. Trellis-sandwich type ilmenite lamellae are common in cubic Ti-magnetite (Fig. 2g). These lamellae indicate the oxy-exsolution of Ti-rich magnetite and into ilmenite and Ti-poor magnetite (e.g., Agarwal et al., 2022; Alva-Valdivia et al., 2017). At the grain boundaries, along fractures and cavities, the Ti-magnetite is sometimes altered to Ti-hematite (Fig. 2h). The Ti-magnetite grains are 50 to 200 m in size. However, they are often marked with the fracture and the lamellae (Fig. 2g) and behave like smaller grains of PSD.
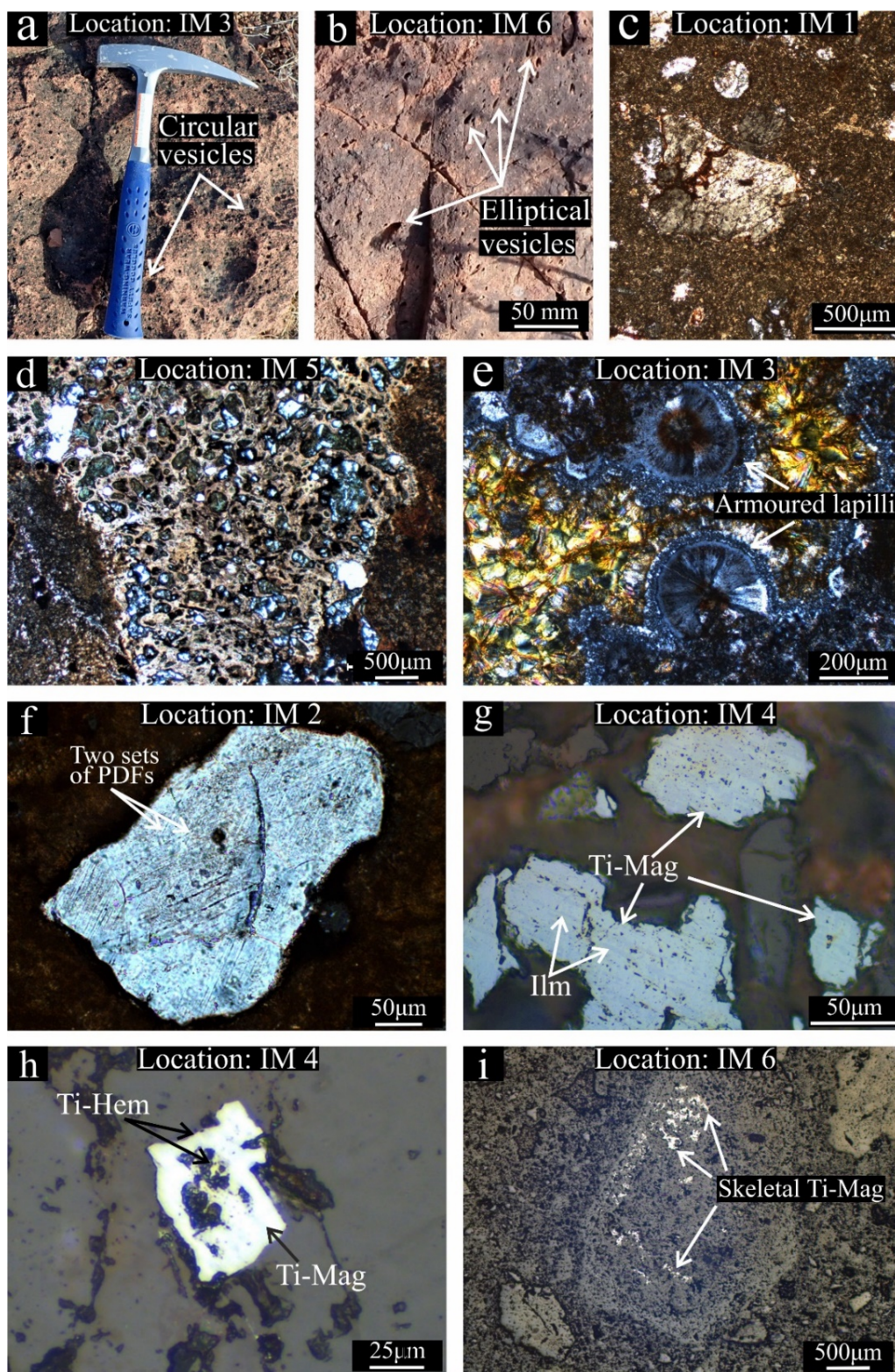
Figure 2: (a, b) Outcrops of IMB containing vesicles. (c-f) Cross polarized images of IMB with poorly sorted clasts-IM1; with fluidal domains of recrystallized feldspar, quartz, and some opaque minerals-IM2; Layered armoured lapilli with authigenic K-feldspar showing an inward-radiating texture surrounded by recrystallized quartz-IM3; Two intersecting sets of PDFs in quartz-IM2. (g-i) Reflected light images showing Ti-magnetite (Ti-Mag) grains with trellis-type ilmenite (Ilm) lamellae-IM4; Cubic Ti-magnetite altered to Ti-hematite (Ti-Hem) along the borders and fractures-IM4; Skeletal Ti-magnetite-IM6.

1.

Rock magnetic properties

(a)

Hysteresis and Day plot

Most of the hysteresis curves are wasp-waisted (Figs. 3a-e), indicating typical low-coercivity ferromagnetic grains. All the sites lie in the PSD region of the Day diagram (Fig. 3f), which suggests a combination of SD and MD behaviour (Dunlop, 2002a). Site 18.1 has the highest single domain component (c. 40%), while site 1 and site 8 have the highest multi-domain component (c. 90%). Mrs/Ms varies from 0.05 to 0.18, and Hcr/Hc from 1.93 to 2.74 (Fig. 3f), revealing the dominance of PSD behaviour. Such PSD behaviour is typical for Ti-magnetite grains of size 50 to 200 m, as are observed under the microscope (Fig. 2g, h). Low saturation and coercivity ratios in the hysteresis curves indicate Ti-poor titanomagnetite.
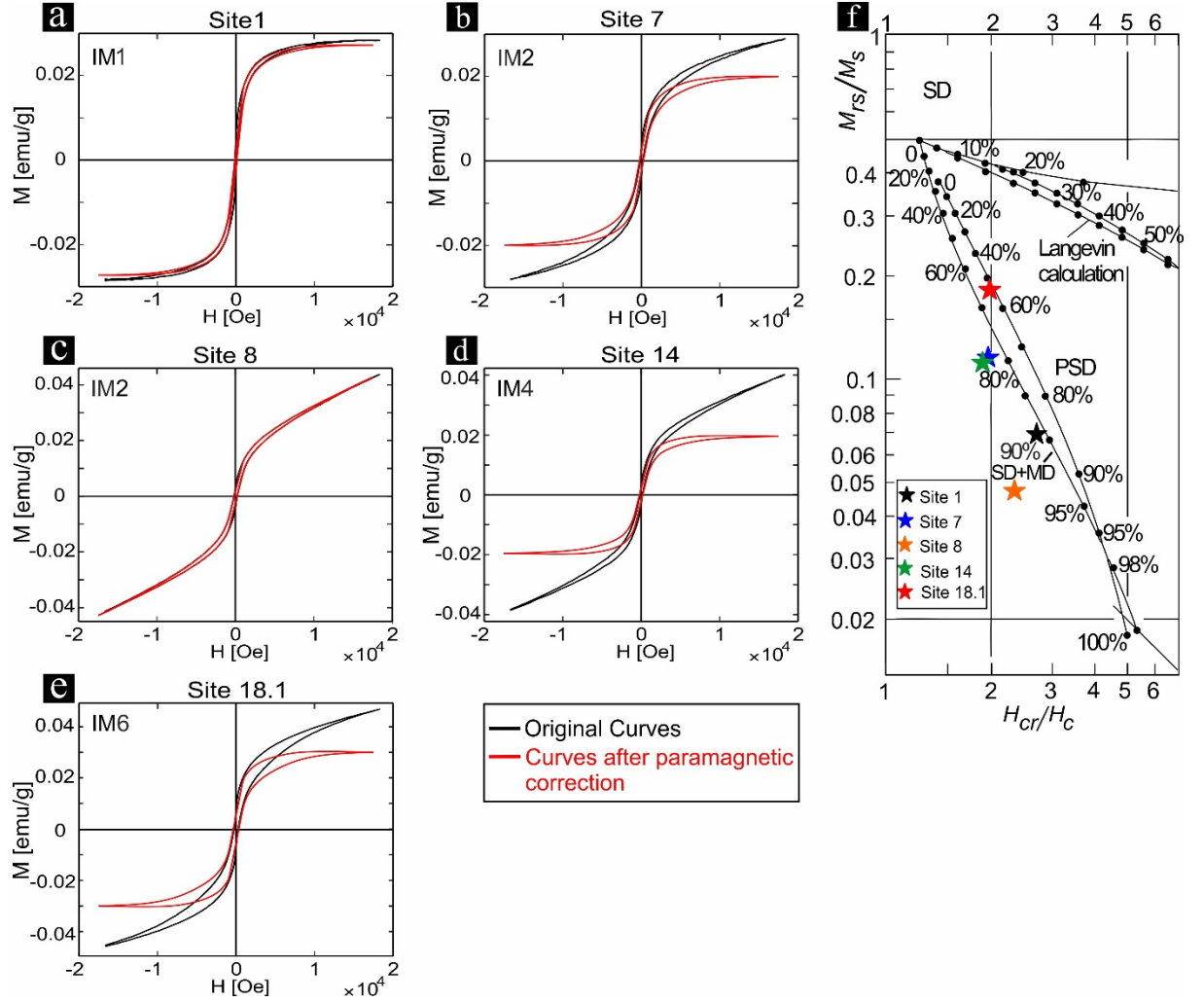
Figure 3: (a-e) Typical hysteresis curves of the Dhala impact melt breccia samples demonstrating variation in magnetization (M) with respect to the magnetic field (H). The wasp-waisted curves indicate the dominance of Pseudo single domain behaviour (f) Day plot (Day et al., 1977; Dunlop, 2002a) elucidating the dominant magnetic domain type in each sample by plotting the ratio of Mrs and Ms against the ratio of Hrs and Hs. The SD, MD, and PSD stand for single domain, multi-domain, and pseudo-single domain, respectively.

Thermomagnetic behaviour

During the low-temperature experiments, the susceptibilities in all the three thermomagnetic curves start to increase gradually from -175°C, achieving a maximum at around -53°C and then subsequently decreasing (Fig. 4). This

may be due to the presence of a metastable ferromagnetic phase in these curves. The subtle peak at -53°C in IM4 is another indication of this metastable phase. Anomalously high susceptibility before -175°C is a measurement artifact from the Kappabridge.

The heating part of the high-temperature curves shows a significant decline in susceptibility between 0° and 100°C, revealing a possible secondary metastable phase with the Currie temperatures (Tc) around 100°C. The second drop in susceptibilities occurs between 550°-600°C in IM1, IM2, and 500°-600°C in IM4, indicating the Tc of titanomagnetite. The variation in Tc of the titanomagnetite may be due to dissimilar proportions of Ti and varying degrees of alterations (e.g., Alva-Valdivia et al., 2019b). All the thermomagnetic curves are irreversible, perhaps due to the presence of metastable phases which transform, during the heating, to ferromagnetic phases with higher susceptibility. The thermomagnetic curve of IM1 exhibit significant noise indicating, in general, low magnetic susceptibility (0.602 to 0.692), which is also evident in the AMS results (Fig. 4, Supplementary Table 1).
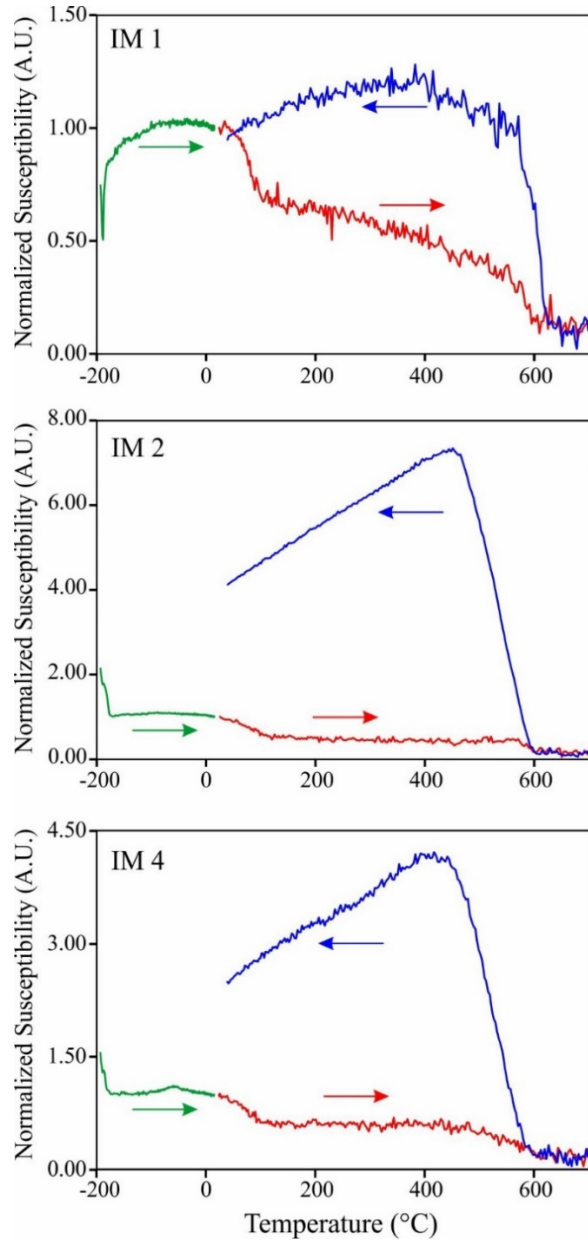
Figure 4: Variations in normalized magnetic susceptibility (A.U. - arbitrary units) with temperature (°C) in the representative samples of Dhala impact melt breccia. Susceptibility is normalized with respect to susceptibility at room temperature. The green curve is obtained during the low-temperature experiment, while the red and blue curves are obtained during the heating and cooling phases of the high-temperature experiment, respectively.

AMS results

The bulk magnetic susceptibility ranges between 0.5×10^{-3} and 2.5×10^{-3} SI units, thus indicating ferri + paramagnetic contribution (Supplementary Table 1). At a few sites (2, 3, 11, and 18.1), the principal susceptibility axes are well-clustered with a triaxial distribution (Fig. 1). The triaxial arrangement is weaker for sites 8, 10, 14, and 15. The magnetic fabrics at these sites vary from mostly oblate (sites 2, 8, 10, and 14) to almost neutral (sites 15 and 18.1) to prolate (sites 3 and 11). Contrary to the triaxial arrangement, sites 1, 7, and 18.2 present well-foliated oblate to neutral magnetic fabrics with K_1 and K_2 falling in a girdle (Table 1). P' ranges from 1.002-1.033, indicating a weakly anisotropic fabric (Supplementary Table 1).

K_m and the P' do not show any relationship and are independent of one another (Supplementary Fig. 1a). For example, the K_m remains almost constant as the P' increases for sites 1 and 18. Most probably the corrected degree of anisotropy (P') is controlled by the paramagnetic minerals. This control is further substantiated by the linear relation between T and P' (Supplementary Fig. 1b).

The mean magnetic lineation, represented by mean K_1, trends between NNW and SSW at all sites except for 18.2 (Table 1, Supplementary Fig. 2) and has shallow to steep plunge (4° to 68°). Except at sites 8, 14, and 15, K_3 are well clustered with a confidence angle below 25°. K_3 trends towards SE for all sites except for 15 and 18.1 and are shallow to steeply plunging, 5° to 85° (Table 1). Thus, the mean magnetic foliation trends almost NE-SW with shallow to steep dips.

1.

Discussions

(a)

Westward flow directions from the magnetic fabrics

Microscopic, thermomagnetic, and magnetic fabrics reveal that the PSD grains of Ti-poor magnetite and Ti-hematite are the magnetic carriers in the IMB (Figs. 2g and h). Ti-magnetite grains are often decorated with trellis-type lamellae of ilmenite (Fig. 2g). The skeletal Ti-magnetite grains (Fig. 2i) and the dendritic and spherulitic texture of silicates (Fig. 2e) indicate rapid cooling and crystallization from the impact melt (Agarwal et al., 2017; Alva-Valdivia et al., 2019a; Osinski, 2004). In contrast, the cubic grains of Ti-magnetite demonstrate slower cooling. This may be due to variable cooling rates at various IMB outcrops.

The mesoscopic flow indicators in 10 specimens collected from 5 different sites were compared with the orientations of K_1, K_2, and K_3 to identify the principal susceptibility axis that defines the flow direction in IMB. In all the compared cases, K_1 aligns with the flow indicators. At all sites except (15 and 18.1), the magnetic foliation strikes almost NE-SW. While the K_1 trends generally westward (ranging between NW to SW) at all sites except site 18.2, where it is oriented towards SE (Supplementary Fig. 2). We, therefore, suggest that the general flow direction of the IMB was westward.

Within most IMB outcrops, the K_1 orientation shows some misalignment, indicating variation in the flow directions. These may be due to slight changes in the slope, flow velocity, and trajectory (e.g., Cañón-Tapia et al., 1996, 1995; Guimarães et al., 2018; Henry et al., 2003; Knight and Walker, 1988; Zhang et al., 2011). Site 18.2 from outcrop IM6 presents K_1 towards SE (Supplementary Fig. 2), which is quite different from the westward K_1 at site 18.1 of the same outcrop. The two sites were only a few meters apart. We owe the anomalous orientation of mean K_1 (declination of 129°) at site 18.2 to the fact that the magnetic fabrics are almost neutral with mean T = -0.06 as the mean intensities of K_1 and K_2 are the same (Table 1, Supplementary Table 1). The K_1 and K_2 are thus, interchangeable. Mean K_2 trends almost westward. The orientation of K_1 and K_2 are thus, switched at site 18.2 compared with 18.1 due to the neutral fabric and interchangeability of the two axes (Table 1, Supplementary Table 1).

Singh et al. (2021a) have examined the magnetic fabrics from the five IMB outcrops, which correspond to our IM1, IM2, IM3, IM4, IM5, and IM6. They most probably considered IM4 and IM5 as one. Their K_m and P' values are close to ours. Moreover, in a few cases, their K_1 parallels the geological flow indicators, which is consistent with our results. However, they describe the magnetic fabrics as poorly defined and scattered without any consistency. It is likely that a large clast population in their samples may have affected the magnetic fabrics, as is common with volcanic pyroclastic deposits (e.g., Alva-Valdivia et al., 2017; Cañón-Tapia and Mendoza-Borunda, 2014).

Ballistic ejection followed by surficial pyroclastic flow emplacement

Impact melt formation and its subsequent emplacement are the primary characteristics of hypervelocity impacts events (Dressler and Reimold, 2001; Osinski et al., 2011). Therefore, the origin and emplacement of impact melt are crucial for planetary exploration. In the present investigation of the IMB, the magnetic lineations are well developed, and interpreted flow directions are generally westward. We thus, propose that, during the emplacement, the IMB was in the semi-molten state with at least some crystallized Ti-magnetite grains, and the temperature was below the melting point of Ti-magnetite, c. 1500°C. If the IMB had been completely molten without magnetic crystals and the solidi-

fication started after the emplacement, there would not have been a consistent trend of magnetic lineation. Furthermore, if the grains in IMB were already solid before emplacement, there would not be microscopic flow textures, and the magnetic foliation and lineation would be chaotic.

The strong clustering of the principal susceptibility axes, observed at a few sites (sites 2, 3, 10, 11, and 18.1 in Fig. 1) indicates a laminar flow, whereas the weak clustering at a few sites (sites 8, 14, and 15 in Fig. 1) reveals turbulent flow (e.g., Cañón-Tapia et al., 1996, 1995; Henry et al., 2003). At the same time, the poorly sorted clasts noticed in the thin sections (Fig. 2c), which are the typical features of IMB (e.g., Pati et al., 2017), suggest a surficial flow of the IMB rather than its airborne emplacement (Osinski et al., 2011). We draw this conclusion based on several studies of impact melt at Ries Crater, Germany, which argue that the impact melt containing poorly sorted clasts is the typical characteristic of the emplacement as a surface flow after the ballistic ejection (e.g., Bringemeier, 1994; Osinski et al., 2011). Besides Ries crater, surficial flows after the ballistic ejection are a common occurrence at several other terrestrial impacts structures, such as the Haughton structure, Canada (Osinski et al., 2005), Barringer, USA (Grant and Schultz, 1993), and Lonar, India (Maloof et al., 2010).

After the initial ballistic ejection, the semi-molten IMB moved as surface flow, either similar to pyroclastic flows or as ground-hugging volatile- and melt-rich flows (e.g., Bringemeier, 1994; Osinski et al., 2011). In the case of volcanic deposits, melt-rich flows such as the flood basalts are characterized by steeply plunging K_3 and shallow dipping magnetic fabrics (e.g., Emry et al., 2014; Sangode et al., 2017); in contrast, pyroclastic flows have variably plunging K_3 with magnetic fabrics presenting a range of dip amounts (e.g., Alva-Valdivia et al., 2017; Cañón-Tapia and Mendoza-Borunda, 2014). Similar to the pyroclastic deposits, the IMB also shows variably plunging K_3 (Table 1). It is, therefore, likely that the emplacement of the IMB was more similar to pyroclastic flows than ground-hugging flows.

Westward direction of impact

All the IMB outcrops at the Dhala impact structure are located NE to W of the central elevated area (Fig. 1). There is no IMB outcrops in E and S directions. This may be due to an east-to-west directed impactor, as oblique impacts are known to produce an asymmetrically stronger distribution of the ejecta and melt in the downrange (e.g., Osinski, 2004; Pierrazzo and Melosh, 2000). However, this asymmetric distribution may also be a consequence of the deep erosion suffered by the Dhala impact structure. Another argument in favour of the westward impact direction is that oblique impacts (impact angle < 50°) create downrange momentum-driven asymmetric flow, which is contrary to radially outward with symmetric flow fields in a vertical impact (Anderson and Schultz, 2006; Pierrazzo and Melosh, 2000). The IMB presents consistent

westward flow vectors suggesting asymmetric excavation flow fields towards the west. This indicates that the impactor at Dhala travelled from east to west and struck at an impact angle below 50°.

Conclusions

The present study combines mesoscopic and magnetic fabrics studies from the Dhala impact structure to investigate the emplacement setting of the IMB. The general trend of magnetic lineation is westward, indicating that the IMB flowed towards the west. The magnetic fabrics dips vary among individual specimens from a site, indicating the IMB moved as a pyroclastic-like flow with a temperature below c. 1500°C (melting point of Ti-magnetite). The presence of poorly sorted clasts indicates the IMB emplacement as surficial flow. We conclude that the IMB was in a semi-molten state after the ballistic ejection and moved as the surficial pyroclastic-like flow rather than a volatile- and melt-rich ground-hugging flow. Based on the interpreted flow vectors, we suggest that the Dhala impact structure was formed by east to west directed impactor that struck an angle of less than 50°.

Acknowledgments

Data Availability Statement

The authors confirm that all the data supporting the findings of this study are available within the article and in the supplementary files submitted. The data presented here is all new and generated during the current study. The AMS data were obtained and processed through Anisoft- 5.1.08 software (Chadima and Jelinek, 2009; Tarling and Hrouda, 1993) which is open source and freely available at https://www.agico.com/text/software/anisoft/anisoft.php

A MATLAB-based software package called HystLab (Paterson et al., 2018) was used for the paramagnetic correction of the hysteresis data and to calculate the coercive force (Hc), the remanent-magnetization (Mrs), and saturation-magnetization (Ms). The HystLab software package is freely available at https://github.com/greigpaterson/HystLab.

References

Agarwal, A., Alva-Valdivia, L.M., Hernández-Cardona, A., Shukla, R.A., Joshi, G., Agarwal, K.K., 2022. Tectonics, cooling rates and temperatures during emplacement of the Rajmahal traps, India. J. Volcanol. Geotherm. Res. 424. https://doi.org/10.1016/j.jvolgeores.2022.107496Agarwal, A., Alva-Valdivia, L.M., Rivas-Sánchez, M.L., Herrero-Bervera, E., Urrutia-Fucugauchi, J., Espejel-García, V., 2017. Emplacement dynamics and hydrothermal alteration of the Atengo ignimbrite, southern Sierra Madre Occidental, northwestern Mexico. J. South Am. Earth Sci. 80, 559–568. https://doi.org/10.1016/j.jsames.2017.10.017Agarwal, A., Kontny, A., Srivastava, D.C., Greiling, R.O., 2016. Shock pressure estimates in target basalts of a pristine crater: A case study in the lonar crater, India. Bull. Geol. Soc. Am. 128, 19–28. https://doi.org/10.1130/B31172.1Agarwal, A., Kumar, S., Joshi, G., Agarwal, K.K., 2020. Evidence for shock provides insight into the formation of the central elevated area in the Dhala impact structure, India. Meteorit. Planet. Sci. 55, 2772–2779. https://doi.org/10.1111/maps.13604Alva-Valdivia, L.M., Agarwal, A., Caballero-Miranda, C., García-Amador, B.I., Morales-Barrera, W., Rodríguez-Elizarraráz, S., Rodríguez-Trejo, A., 2017. Paleomagnetic and AMS studies of the El Castillo ignimbrite, central-east Mexico: Source and rock magnetic nature. J. Volcanol. Geotherm. Res. 336, 140–154. https://doi.org/10.1016/j.jvolgeores.2017.02.014Alva-Valdivia, L.M., Rodríguez-Trejo, A., Morales, J., González-Rangel, J.A., Agarwal, A., 2019a. Paleomagnetism and age constraints of historical lava flows from the El Jorullo volcano, Michoacán, Mexico. J. South Am. Earth Sci. 93, 439–448. https://doi.org/10.1016/j.jsames.2019.05.016Alva-Valdivia, L.M., Rodríguez-Trejo, A., Vidal-Solano, J.R., Paz-Moreno, F., Agarwal, A., 2019b. Emplacement temperature resolution and age determination of Cerro Colorado tuff ring by paleomagnetic analysis, El Pinacate Volcanic Field, Sonora, Mexico. J. Volcanol. Geotherm. Res. 369, 145–154. https://doi.org/10.1016/j.jvolgeores.2018.11.012Anderson, J.L.B., Schultz, P.H., 2006. Flow-field center migration during vertical and oblique impacts. Int. J. Impact Eng. 33, 35–44. https://doi.org/10.1016/j.ijimpeng.2006.09.022Barlow, N.G., 2010. What we know about Mars from its impact craters. Bull. Geol. Soc. Am. 122, 644–657. https://doi.org/10.1130/B30182.1Bringemeier, D., 1994. Petrofabric examination of the main suevite of the Otting Quarry, Nordlinger Ries, Germany. Meteoritics 29, 417–422. https://doi.org/10.1111/j.1945-5100.1994.tb00607.xCañón-Tapia, E. and Castro, J., 2004. AMS measurements on obsidian from the Inyo Domes, CA: a comparison of magnetic and mineral preferred orientation fabrics 134, 169–182. https://doi.org/10.1016/j.jvolgeores.2004.01.005Cañón-Tapia, E., Mendoza-Borunda, R., 2014. Magnetic petrofabric of igneous rocks: Lessons from pyroclastic density current deposits and obsidians. J. Volcanol. Geotherm. Res. 289, 151–169. https://doi.org/10.1016/j.jvolgeores.2014.11.006Cañón-Tapia, E., Walker, G.P.L., Herrero-bervera, E., 1997. The internal structure of lava flows-insights from AMS measurements II: Hawaiian pahoehoe, toothpaste lava and 'a'ā. J. Volcanol. Geotherm. Res. 19–46.Cañón-Tapia, E., Walker,

G.P.L., Herrero-bervera, E., 1996. The internal structure of lava flows-insights from AMS measurements I : Near-vent a' a. J. Volcanol. Geotherm. Res. 21–36.Cañón-Tapia, E., Walker, G.P.L., Herrero-bervera, E., 1995. Magnetic fabric and flow direction in basaltic Pahoehoe lava of Xitle Volcano , Mexico. J. Volcanol. Geotherm. Res. 65, 249–263.Chadima, M., Jelinek, V., 2009. Anisoft 4.2. Anisotropy Data Browser for Windows. Agico.Day, R., Fuller, M., Schmidt, V.A., 1977. Hysteresis properties of titanomagnetites: Grain-size and compositional dependence. Phys. Earth Planet. Inter. 13, 260–267. https://doi.org/10.1016/0031-9201(77)90108-XDressler, B.O., Reimold, W.U., 2001. Terrestrial impact melt rocks and glasses. Earth-Science Rev. 56, 205–284. https://doi.org/10.1016/S0012-8252(01)00064-2Dunlop, D.J., 2002a. Theory and application of the Day plot (Mrs/Ms versus Hcr/Hc) 1. Theoretical curves and tests using titanomagnetite data. J. Geophys. Res. 107, 1–15. https://doi.org/10.1029/2001jb000486Dunlop, D.J., 2002b. Theory and application of the Day plot (Mrs/Ms versus Hcr/Hc) 2. Application to data for rocks, sediments, and soils. J. Geophys. Res. 107, 1–22. https://doi.org/10.1029/2001jb000487Ellwood, B.B., 1978. Flow and emplacement direction determined for selected basaltic bodies using magnetic susceptibility anisotropy measurements 41, 254–264.Emry, E.L., Wiens, D.A., Garcia-Castellanos, D., 2014. Journal of Geophysical Research : Solid Earth. AGU J. Geophys. Res. Solid Earth 119, 3076–3095. https://doi.org/10.1002/2013JB010660.ReceivedFrench, B.M., 1998. Traces of Catastrophe: A Handbook of Shock-Metamorphic Effects in Terrestrial Meteorite Impact Structures 120.Gil-Imaz, A., Pocoví, A., Lago, M., Galé, C., Arranz, E., Rillo, C., Guerrero, E., 2006. Magma flow and thermal contraction fabric in tabular intrusions inferred from AMS analysis. A case study in a late-Variscan folded sill of the Albarracín Massif (southeastern Iberian Chain, Spain). J. Struct. Geol. 28, 641–653. https://doi.org/10.1016/j.jsg.2005.12.016Grant, J.A., Schultz, P.H., 1993. Degradation of selected terrestrial and Martian impact craters. J. Geophys. Res. 98. https://doi.org/10.1029/93je00121Grieve, R.A.F., 2005. Economic natural resource deposits at terrestrial impact structures. Geol. Soc. London, Spec. Publ. 248, 1–29. https://doi.org/10.1144/GSL.SP.2005.248.01.01Guimarães, L.F., Raposo, M.I.B., Janasi, V.A., Cañón-tapia, E., Polo, L.A., 2018. An AMS study of different silicic units from the southern Paraná-Etendeka Magmatic Province in Brazil: Implications for the identification of flow directions and local sources. J. Volcanol. Geotherm. Res. 355, 304–318. https://doi.org/10.1016/j.jvolgeores.2017.11.014Henry, B., Plenier, G., Camps, P., 2003. Post-emplacement tilting of lava flows inferred from magnetic fabric study: The example of Oligocene lavas in the Jeanne d'Arc Peninsula (Kerguelen Islands). J. Volcanol. Geotherm. Res. 127, 153–164. https://doi.org/10.1016/S0377-0273(03)00198-7Jelínek, V. and Kropáček, V., 1978. Statistical processing of anisotropy of magnetic susceptibility measured on groups of specimens. 50–62.Khan, M.A., 1962. The anisotropy of magnetic susceptibility of some igneous and metamorphic rocks. J. Geophys. Res. 67, 2873–2885. https://doi.org/10.1029/jz067i007p02873Knight, M.D., Walker,

G.P.L., 1988. Magma flow directions in dikes of the Koolau complex, Oahu, determined from magnetic fabric studies (Hawaii). J. Geophys. Res. 93, 4301–4319. https://doi.org/10.1029/JB093iB05p04301Kring, D.A., 2000. Impact events and their effect on the origin, evolution, and distribution of life. GSA today 10, 1–7.Liu, B., Saito, Y., Yamazaki, T., Abdeldayem, A., Oda, H., Hori, K., Zhao, Q., 2001. Paleocurrent analysis for the Late Pleistocene-Holocene incised-valley fill of the Yangtze delta, China by using anisotropy of magnetic susceptibility data. Mar. Geol. 176, 175–189. https://doi.org/10.1016/S0025-3227(01)00151-7MacDonald, W. D. and Palmer, H.C., 1990. Flow directions in ash-flow tuffs: a comparison of geological and magnetic susceptibility measurements, Tshirege member (upper Bandelier Tuff), Valles caldera, New Mexico, USA. Bull. Volcanol. 53, 45–59.Mader, M.M., Osinski, G.R., 2018. Impactites of the Mistastin Lake impact structure: Insights into impact ejecta emplacement. Meteorit. Planet. Sci. 53, 2492–2518. https://doi.org/10.1111/maps.13173Maloof, A.C., Stewart, S.T., Weiss, B.P., Soule, S.A., Swanson-Hysell, N.L., Louzada, K.L., Garrick-Bethell, I., Poussart, P.M., 2010. Geology of Lonar Crater, India. Bull. Geol. Soc. Am. 122, 109–126. https://doi.org/10.1130/B26474.1Osinski, G.R., 2004. Impact melt rocks from the Ries structure, Germany: an origin as impact melt flows? 226, 529–543. https://doi.org/10.1016/j.epsl.2004.08.012Osinski, G.R., Cockell, C.S., Pontefract, A., Sapers, H.M., 2020. The Role of Meteorite Impacts in the Origin of Life. Astrobiology 20, 1121–1149. https://doi.org/10.1089/ast.2019.2203Osinski, G.R., Spray, J.G., Lee, P., 2005. Impactites of the Haughton impact structure, Devon Island, Canadian High Arctic. Meteorit. Planet. Sci. 40, 1789–1812. https://doi.org/10.1111/j.1945-5100.2005.tb00147.xOsinski, G.R., Tornabene, L.L., Banerjee, N.R., Cockell, C.S., Flemming, R., Izawa, M.R.M., McCutcheon, J., Parnell, J., Preston, L.J., Pickersgill, A.E., Pontefract, A., Sapers, H.M., Southam, G., 2013. Impact-generated hydrothermal systems on Earth and Mars. Icarus 224, 347–363. https://doi.org/10.1016/j.icarus.2012.08.030Osinski, G.R., Tornabene, L.L., Grieve, R.A.F., 2011. Impact ejecta emplacement on terrestrial planets. Earth Planet. Sci. Lett. 310, 167–181. https://doi.org/10.1016/j.epsl.2011.08.012Papanna, G., Venkateshwarlu, M., Periasamy, V., Nagendra, R., 2014. Anisotropy of magnetic susceptibility (AMS) studies of Campanian-Maastrichtian sediments of Ariyalur Group, Cauvery Basin, Tamil Nadu, India: An appraisal to Paleocurrent directions. J. Earth Syst. Sci. 123, 351–364. https://doi.org/10.1007/s12040-013-0400-1Paterson, G.A., Zhao, X., Jackson, M., Heslop, D., 2018. Measuring, Processing, and Analyzing Hysteresis Data. Geochemistry, Geophys. Geosystems 19, 1925–1945. https://doi.org/10.1029/2018GC007620Pati, J.K., Jourdan, F., Armstrong, R.A., Reimold, W.U., Prakash, K., 2010. First SHRIMP U-Pb and $^{40}Ar/^{39}Ar$ chronological results from impact melt breccia from the Paleoproterozoic Dhala impact structure, India. Spec. Pap. Geol. Soc. Am. 465, 571–591. https://doi.org/10.1130/2010.2465(27)Pati, J.K., Poelchau, M.H., Reimold, W.U., Nakamura, N., Kuriyama, Y., Singh, A.K., 2019. Documentation of shock features in impactites from the Dhala impact structure, India. Meteorit.

Planet. Sci. 54, 2312–2333. https://doi.org/10.1111/maps.13369Pati, J.K., Qu, W.J., Koeberl, C., Reimold, W.U., Chakarvorty, M., Schmitt, R.T., 2017. Geochemical evidence of an extra-terrestrial component in impact melt breccia from the Paleoproterozoic Dhala impact structure, India. Meteorit. Planet. Sci. 52, 722–736. https://doi.org/10.1111/maps.12826Pati, J.K., Reimold, W.U., Greshake, A., Schmitt, R.T., Koeberl, C., Pati, P., Prakash, K., 2015. Pseudotachylitic breccia from the Dhala impact structure, north-central India: Texture, mineralogy and geochemical characterization. Tectonophysics 649, 18–32. https://doi.org/10.1016/j.tecto.2015.01.021Pati, J.K., Reimold, W.U., Koeberl, C., Pati, P., 2008. The Dhala structure, Bundelkhand craton, Central India - Eroded remnant of a large Paleoproterozoic impact structure. Meteorit. Planet. Sci. 43, 1383–1398. https://doi.org/10.1111/j.1945-5100.2008.tb00704.xPierrazzo, E., Melosh, H.J., 2000. Understanding oblique impacts from experiments, observations, and modeling. Annu. Rev. Earth Planet. Sci. 141–167.Ray, J.S., Veizer, J., Davis, W.J., 2003. C, O, Sr and Pb isotope systematics of carbonate sequences of the Vindhyan Supergroup, India: Age, diagenesis, correlations and implications for global events. Precambrian Res. 121, 103–140. https://doi.org/10.1016/S0301-9268(02)00223-1Reddy, S.M., Johnson, T.E., Fischer, S., Rickard, W.D.A., Taylor, R.J.M., 2015. Precambrian reidite discovered in shocked zircon from the Stac Fada impactite, Scotland. Geology 43, 899–902. https://doi.org/10.1130/G37066.1Reimold, W.U., Koeberl, C., Gibson, R.L., Dressler, B.O., 2005. Economic Mineral Deposits in Impact Structures: A Review, Impact Tectonics. https://doi.org/10.1007/3-540-27548-7_20Sangode, S.J., Sharma, R., Mahajan, R., Basavaiah, N., Srivastava, P., Gudadhe, S.S., Meshram, D.C., Venkateshwarulu, M., 2017. Anisotropy of magnetic susceptibility and rock magnetic applications in the Deccan volcanic province based on some case studies. J. Geol. Soc. India 89, 631–642. https://doi.org/10.1007/s12594-017-0672-1Sarangi, S., Gopalan, K., Kumar, S., 2004. Pb-Pb age of earliest megascopic, eukaryotic alga bearing Rohtas Formation, Vindhyan Supergroup, India: Implications for Precambrian atmospheric oxygen evolution. Precambrian Res. 132, 107–121. https://doi.org/10.1016/j.precamres.2004.02.006Siegert, S., Branney, M.J., Hecht, L., 2017. Density current origin of a melt-bearing impact ejecta blanket (Ries suevite, Germany). Geology 45, 855–858. https://doi.org/10.1130/G39198.1Singh, A.K., Pati, J.K., Patil, S.K., Reimold, W.U., Rao, A.K., Pandey, O.P., 2021a. Anisotropy of magnetic susceptibility (AMS) of impact melt breccia and target rocks from the Dhala impact structure, India, in: Reimold, W.U., Koeberl, C. (Eds.), Large Meteorite Impacts and Planetary Evolution VI. Geological Society of America, pp. 351–371. https://doi.org/10.1130/2021.2550(14)Singh, A.K., Pati, J.K., Sinha, R., Reimold, W.U., Prakash, K., Nadeem, M., Dwivedi, S., Mishra, D., Dwivedi, A.K., 2021b. Characteristic landforms and geomorphic features associated with impact structures: Observations at the Dhala structure, north-central India. Earth Surf. Process. Landforms 46, 1482–1503. https://doi.org/10.1002/esp.5115Stöffler, D., Artemieva, N.A., Ivanov, B.A.,

Hecht, L., Kenkmann, T., Schmitt, R.T., Tagle, R.A., Wittmann, A., 2004. Origin and emplacement of the impact formations at Chicxulub, Mexico, as revealed by the ICDP deep drilling at Yaxcopoil-1 and by numerical modeling. Meteorit. Planet. Sci. 39, 1035–1067. https://doi.org/10.1111/j.1945-5100.2004.tb01128.xStopar, J.D., Hawke, B.R., Robinson, M.S., Denevi, B.W., Giguere, T.A., Koeber, S.D., 2014. Occurrence and mechanisms of impact melt emplacement at small lunar craters. Icarus 243, 337–357. https://doi.org/10.1016/j.icarus.2014.08.011Sugandhi, E., Agarwal, A., 2022. Jet onset time and velocity for various natural hypervelocity impacts. Int. J. Impact Eng. 168, 104310. https://doi.org/10.1016/j.ijimpeng.2022.104310Tarling, D.H., and Hrouda, F., 1993. The magnetic anisotropy of rocks, TectonophysicsLondon, UK, Chapman and Hall. https://doi.org/6Tauxe, L., Mullender, T.A.T., Pick, T., 1996. Potbellies, wasp-waists, and superparamagnetism in magnetic hysteresis. J. Geophys. Res. Solid Earth 101, 571–583. https://doi.org/10.1029/95jb03041Zhang, S., Cañón-tapia, E., Walderhaug, H.J., 2011. Magnetic fabric and its significance in the sills and lava flows from Taimyr fold-belt, Arctic Siberia. Tectonophysics 505, 68–85. https://doi.org/10.1016/j.tecto.2011.04.004

23